JACS
JOURNAL OF THE AMERICAN CHEMICAL SOCIETY

pubs.acs.org/JACS

Article

Revealing the Role of CO during CO_2 Hydrogenation on Cu Surfaces with *In Situ* Soft X-Ray Spectroscopy

Jack E. N. Swallow, Elizabeth S. Jones, Ashley R. Head, Joshua S. Gibson, Roey Ben David, Michael W. Fraser, Matthijs A. van Spronsen, Shaojun Xu, Georg Held, Baran Eren,* and Robert S. Weatherup*

Cite This: *J. Am. Chem. Soc.* 2023, 145, 6730–6740

Read Online

ACCESS | Metrics & More | Article Recommendations | Supporting Information

ABSTRACT: The reactions of H_2, CO_2, and CO gas mixtures on the surface of Cu at 200 °C, relevant for industrial methanol synthesis, are investigated using a combination of ambient pressure X-ray photoelectron spectroscopy (AP-XPS) and atmospheric-pressure near edge X-ray absorption fine structure (AtmP-NEXAFS) spectroscopy bridging pressures from 0.1 mbar to 1 bar. We find that the order of gas dosing can critically affect the catalyst chemical state, with the Cu catalyst maintained in a metallic state when H_2 is introduced prior to the addition of CO_2. Only on increasing the CO_2 partial pressure is CuO formation observed that coexists with metallic Cu. When only CO_2 is present, the surface oxidizes to Cu_2O and CuO, and the subsequent addition of H_2 partially reduces the surface to Cu_2O without recovering metallic Cu, consistent with a high kinetic barrier to H_2 dissociation on Cu_2O. The addition of CO to the gas mixture is found to play a key role in removing adsorbed oxygen that otherwise passivates the Cu surface, making metallic Cu surface sites available for CO_2 activation and subsequent conversion to CH_3OH. These findings are corroborated by mass spectrometry measurements, which show increased H_2O formation when H_2 is dosed before rather than after CO_2. The importance of maintaining metallic Cu sites during the methanol synthesis reaction is thereby highlighted, with the inclusion of CO in the gas feed helping to achieve this even in the absence of ZnO as the catalyst support.

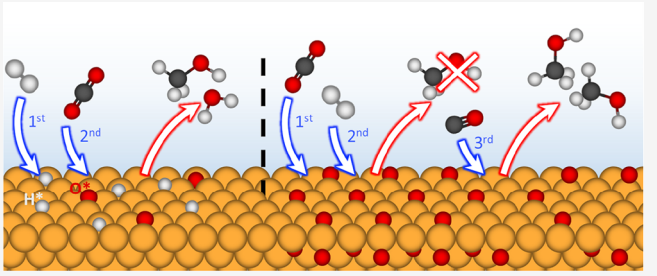

INTRODUCTION

The decarbonization of industrial processes is central to reducing global CO_2 emissions and current societal reliance on unevenly distributed fossil fuel resources. Methanol synthesis by hydrogenation of CO_2 offers a means of utilizing captured CO_2 that, when combined with H_2 produced by electrochemical water splitting, yields zero or even negative carbon emissions, as long as the required energy input comes from renewable sources. Global methanol consumption has risen dramatically in recent decades from ~5 Mt/year in 1975 up to ~107 Mt/year in 2021, with the majority used as feedstock for the production of important chemical derivatives.[1,2] With an octane number of 113 and a volumetric energy density around half that of gasoline, methanol is also increasingly considered as a direct fuel for internal combustion engines and fuel cells, or indirectly as a liquid carrier for hydrogen.[3−5]

Industrial methanol synthesis is typically performed over Cu-based catalysts at 200−300 °C and 50−100 bar,[5,6] with ~90% of current production based on the conversion of syngas (CO/H_2 mixture, with <20 at. % CO_2) derived from natural gas.[5−10] Although less common, methanol synthesis from CO_2/H_2 has also been industrially implemented, with further plants in development.[5] Despite the change in reaction conditions, $Cu/ZnO/Al_2O_3$ catalysts are typically used in both cases, as well as for the low temperature water gas shift (WGS) reaction. Three key reaction pathways are thus considered in CH_3OH synthesis from $H_2/CO_2/CO$ mixtures (eqs 1, 2, and 3); CO_2 hydrogenation, CO hydrogenation, and WGS.[11]

$$CO_2 + 3H_2 \rightleftharpoons CH_3OH + H_2O \quad \Delta H^\circ = -49\ \text{kJ/mol} \tag{1}$$

$$CO + 2H_2 \rightleftharpoons CH_3OH \quad \Delta H^\circ = -90\ \text{kJ/mol} \tag{2}$$

$$CO + H_2O \rightleftharpoons CO_2 + H_2 \quad \Delta H^\circ = -41\ \text{kJ/mol} \tag{3}$$

Isotope-labelling studies with $Cu/ZnO/Al_2O_3$ catalysts have demonstrated that CH_3OH formation predominantly proceeds via the CO_2 hydrogenation route (eq 1) rather than the much slower direct hydrogenation of CO (eq 2).[12,13] This has been shown to remain the case for unsupported Cu catalysts.[12,14,15]

Received: December 1, 2022
Published: March 14, 2023

https://doi.org/10.1021/jacs.2c12728
J. Am. Chem. Soc. 2023, 145, 6730−6740

Even for a CO-rich feed, CO first undergoes a WGS reaction with H_2O (eq 3) to form CO_2 and H_2, and then CO_2 further reacts with H_2 to yield CH_3OH.[5,16] Using a CO_2-rich feed reduces the need for this additional WGS step; nevertheless, the presence of CO has been implicated in increasing methanol production rate in high conversion conditions.[13] However, the beneficial role of CO remains contentious with several proposed mechanisms including the following: H_2O removal by the WGS reaction (which otherwise kinetically inhibits methanol synthesis), regulation of adsorbed oxygen (O*) on the Cu surface, or reduction of ZnO supports to yield oxygen vacancies or Cu−Zn alloy sites.

CH_3OH formation via the CO_2 hydrogenation route inherently involves the liberation of O ($CO_2 + 2H_2 \rightleftharpoons CH_3OH + O^*$), which goes onto form H_2O in the overall reaction of eq 1 ($O^* + H_2 \rightleftharpoons H_2O$). Similarly, the reverse-WGS reaction (eq 3) liberates O ($CO_2 \rightleftharpoons CO + O^*$), with exposure of Cu surfaces to CO_2 alone, resulting in deactivation due to O* blocking CO_2 adsorption sites.[17] With H_2 present, O* can be removed by H_2O formation, or the addition of CO to the reaction feed can shift the equilibrium, thereby regulating O* coverage. Critical to rationalizing the influence of the reaction feed on methanol productivity is a detailed account of how O* coverage and chemical state of the catalyst surface vary with the balance of reactants under realistic conditions, i.e., approaching the bar-pressure regime used industrially. However, accessing this regime with the required interface sensitivity is a significant challenge due to the dense phases on either side of the solid−gas interface,[18−20] with the majority of reports limited either to bulk-sensitive hard X-ray absorption or pressures below a few mbar.

Herein, we investigate unsupported Cu catalysts using a combination of ambient pressure X-ray photoelectron spectroscopy (AP-XPS) and atmospheric-pressure near edge X-ray absorption fine structure (AtmP-NEXAFS) spectroscopy bridging pressures from 0.1 mbar to 1 bar. We thereby track how the O* coverage and catalyst oxidation state evolve with the composition of the reaction feed at temperatures (200 °C) and pressures (up to 1 bar) more representative of industrial methanol synthesis than prior interface-sensitive studies. For metallic Cu surfaces exposed to H_2, the addition of a similar CO_2 partial pressure leads to O* formation confirming CO_2 activation, but ongoing H_2 activation regulates the O* coverage and suppresses Cu oxidation. However, at high relative CO_2 partial pressures, excess O* leads to Cu oxidation, poisoning the surface against CO_2 and H_2 activation. On removing CO_2, a metallic Cu surface is not recovered, indicating a high kinetic barrier for H_2 activation on Cu_2O. Mass spectrometry (MS) measured at 1 bar corroborates Cu deactivation following CO_2 exposure without H_2 present: A lower H_2O signal is observed when H_2 is reintroduced, indicating that the CO_2 hydrogenation and reverse-WGS reactions are suppressed. The addition of CO to the feed is able to recover metallic sites, which are most active for CO_2 and H_2 activation, allowing methanol generation to proceed. This highlights the important function of CO in industrial methanol synthesis from CO_2-rich feeds, where it serves as a scavenger for adsorbed oxygen preventing saturation of the catalytically active Cu sites and making the process more robust to variations in reaction conditions.

EXPERIMENTAL METHODS

Three morphological variants of the Cu catalyst are used in this study: foil, thin film, and powder. Characterization of their microstructures (see Figures S1−S4) confirms that all can be considered polycrystalline, exhibiting a variety of surface orientations. The techniques used herein therefore probe an ensemble of different Cu surfaces and grain boundaries. Comparisons between the data collected with the different catalyst variants are therefore made within this context. We further note that at the pressures probed in this study, Cu can show significant restructuring.[17,21,22]

AP-XPS in the mbar pressure range was performed at the Center for Functional Nanomaterials at Brookhaven National Laboratory, USA, using a lab-based system from SPECS Surface Nano Analysis GmbH with a PHIOBOS 150 NAP hemispherical analyzer and monochromated Al Kα X-ray source (1486.7 eV).[23] The base pressure of the chamber was ~5 × 10^{-10} mbar. We used polycrystalline Cu foil (Alfa Aesar, 25 μm, 99.999% - metal basis) as a model catalyst, prepared by cycles of conventional *in situ* Ar^+-ion sputtering (1 keV) and annealing (300 °C to remove implanted Ar) until the hydrocarbon signal was below the XPS detection limit. Only Cu, O, and C species were detected at the surface during the experiment. The temperature was measured using a type K thermocouple in contact with the sample surface and was stabilized at 200 °C. H_2, CO_2, and CO were introduced using precision leak valves, with their respective partial pressures indicated in the text below. High-resolution spectra of the Cu 2p, O 1s, and C 1s XP core-levels, Cu LMM Auger−Meitner emission, and the valence band (VB) were collected. The Cu 2p region and VB are only used for energy calibration, with the former exhibiting a negligible difference in XPS binding energy (BE) between the spectra of metallic Cu and Cu_2O.[24] The O 1s and C 1s core-level spectra are fitted with pseudo-Voigt functions and Shirley backgrounds within the CasaXPS software.[25] Auger−Meitner electron spectra (AES) in the Cu LMM region are shown after subtraction of a Shirley background and the wide inelastic feature present on the low kinetic energy side. This subtraction is simply to aid in visualization of the data and has no bearing on data interpretation.

AtmP-NEXAFS measurements at up to 1 bar were performed at beamline B07-C of Diamond Light Source (DLS), UK.[26,27] A custom-designed flow cell was employed that uses an X-ray transparent silicon-nitride (SiN_x) membrane (500 × 500 μm window, 100 nm thick, Silicon-rich nitride, Silson) that can withstand a >1 bar pressure difference (see Figure 1). The cell integrates a type K thermocouple to measure the temperature inside the high-pressure compartment

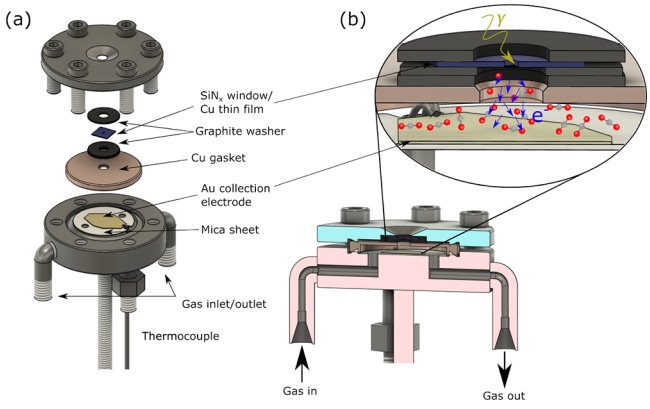

Figure 1. Schematic diagram of cell used for AtmP-NEXAFS spectroscopy. (a) Exploded view showing the arrangement of stacked cell components. (b) Cross section of the assembled cell. The inset shows a magnified schematic indicating the direction of incoming X-rays and generated electrons, with the cell filled with CO_2. The electron yield signal is obtained from the current between the Cu thin film catalyst and the Au collection electrode.

https://doi.org/10.1021/jacs.2c12728
J. Am. Chem. Soc. 2023, 145, 6730−6740

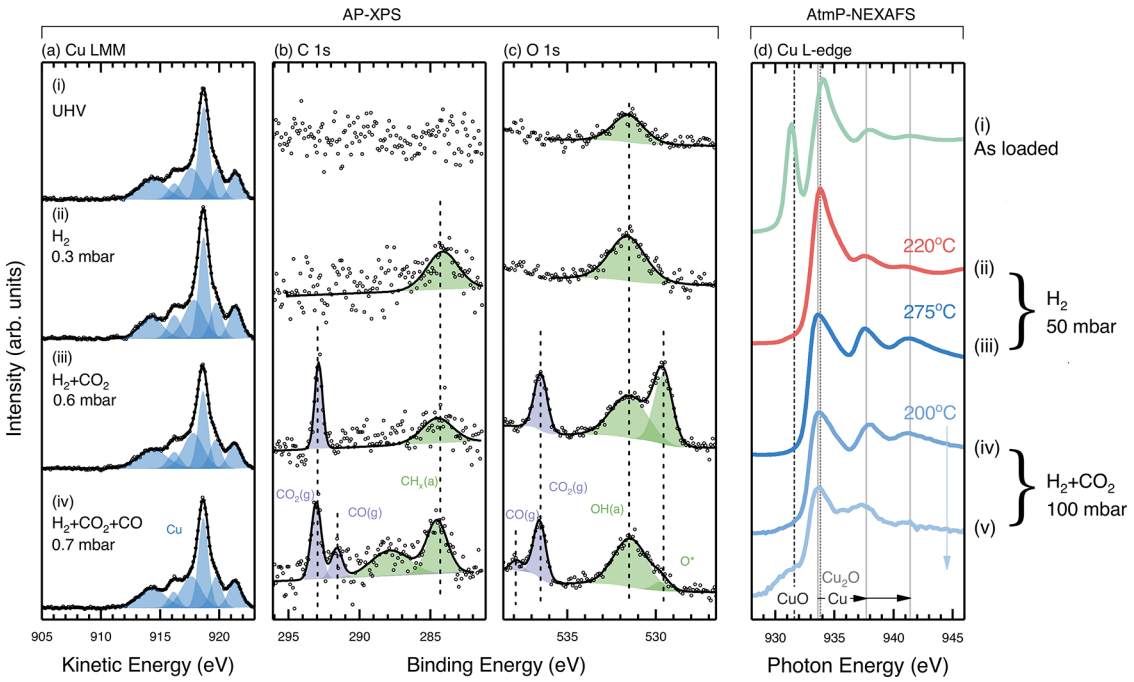

Figure 2. (a–c) Spectra from the Cu LMM, C 1s, and O 1s regions acquired in (i) UHV, (ii) 0.3 mbar H_2, (iii) 0.3 mbar H_2 and 0.3 mbar CO_2, and (iv) 0.3 mbar H_2, 0.3 mbar CO_2 and 0.1 mbar CO. The temperature is fixed at 200 °C for all XP spectra. (d) AtmP-NEXAFS spectra from the Cu L_3-edge acquired (i) for the as-entered sample, (ii) at 220 °C with 50 mbar of H_2, (iii) at 275 °C with 50 mbar H_2, (iv) at 200 °C with 50 mbar of H_2 and 50 mbar of CO_2, and (v) at 200 °C with 25 mbar of H_2 and 75 mbar CO_2.

(temperature reading thermocouple) (see Figure 1a), while an additional mineral-insulated type K thermocouple within a 310 stainless steel probe sheath is wrapped around the outside of the cell and used for resistive heating by applying a current through it (thermocouple for heating). With this design, a stable internal temperature in excess of 420 °C could be reached under vacuum (~340 °C with 1 bar of Ar gas in the cell). The cell housing is made from 304 stainless steel vacuum flanges. An insulating mica sheet is placed on the base flange with a Au foil electrode sitting atop it. The electrode is electrically isolated from the rest of the cell and is contacted through the tip of the temperature reading thermocouple to enable the measurement of drain current. Cu (~60 nm) atop a Cr (~5 nm) adhesion layer was deposited onto the SiN_x membrane by magnetron sputtering to act as the catalyst, and faces the Au electrode within the flow cell. NEXAFS spectroscopy was performed in electron yield (EY) mode by measuring the current between the catalyst film and Au electrode when the catalyst film is under X-ray illumination.[28] Note that AtmP-NEXAFS collected in EY mode has a probing depth of ~10 nm for the Cu L_3-edge collected herein, compared to ~5 nm for the AP-XPS.[20,29] The measurement geometry avoids simultaneous illumination of the Au electrode. The cell is sealed using a copper gasket (modified from a blank gasket by milling a cavity to accommodate the electrode without short-circuiting). A hole through the center of the gasket allows gas to reach the Cu on the SiN_x membrane, which is sealed against the gasket using an expanded graphite washer (Klinger).

The cell was mounted directly onto the B07-C analysis chamber, which includes a differentially-pumped beamline interface mitigating the risk of accidental gas leakage from the cell. Gases are introduced into the cell through 316 stainless steel tubing (see Figure 1b), with their flow controlled by mass flow controllers (MFCs) on the inlet and a variable pumping valve on the outlet. The pressure of the gases within the cell was monitored using a combination of capacitance (up to 100 mbar) and Bourdon-tube gauges (up to 1 bar). X-rays in the energy range of 250–2800 eV could be selected, allowing for measurements of Cu L_3-, O K-, and C K-edges to be taken. The beamline exit slits were opened to 500 μm in the non-dispersive direction and 50 μm in the dispersive direction, which resulted in a spot size of approximately 90 μm × 100 μm.[27] All AtmP-NEXAFS spectra are shown after subtracting a linear background fitted to the pre-edge region and post-edge normalization. Absolute energy calibration was performed using the metallic Cu catalyst obtained by H_2 annealing (main peak set to 933.7 eV).[30]

MS measurements were performed at the Research Complex at Harwell (RCaH) using a Hiden Analytical Catlab microreactor module coupled with a quartz inert capillary continuous sampling mass spectrometer. Mass spectra of gas-phase products were recorded in a geometry consisting of a plug-flow reactor and a quadrupole MS. 150 mg of Cu powder (Alfa Aesar, −100 mesh (≤150 μm), 99%) was placed in a quartz tube (5 mm inner diameter) between two plugs of quartz wool. Cu powder was used here as a model catalyst due to the increased surface area available compared to bulk foil, thus increasing the yield of reaction products. Gas flow into the reactor was controlled using MFCs, where the total flow of gases was held at 50 standard cubic cm (sccm). Ar was used to balance the gas flow upon changing the composition of the input gas, helping to reduce fluctuations in partial pressure of each component. Atmospheric pressure was maintained within the reactor throughout the experiment. The sample was initially pretreated by introducing H_2 (20 sccm) and annealing at 275 °C for 1 h; the Cu was determined to be fully reduced once the H_2O signal decreased to a stable value and this was confirmed by ex situ AES following inert transfer (see Figure S5). The composition of gas flow into the microreactor was then varied sequentially using $H_2/CO_2/CO$ mixtures.

RESULTS AND DISCUSSION

Figure 2a–c shows the collected XP spectra for the polycrystalline Cu surface during sequential exposure to different $H_2/CO_2/CO$ mixtures at 200 °C. The chemical state of the Cu surface is obtained by fitting AES of the Cu LMM region shown in Figure 2a using similar line-shapes (peak position and width) as those in ref 24 to fit Cu and Cu_2O mixtures. Peaks corresponding to metallic Cu are shown in blue, whereas those related to Cu_2O are shown in red (only

https://doi.org/10.1021/jacs.2c12728
J. Am. Chem. Soc. 2023, 145, 6730–6740

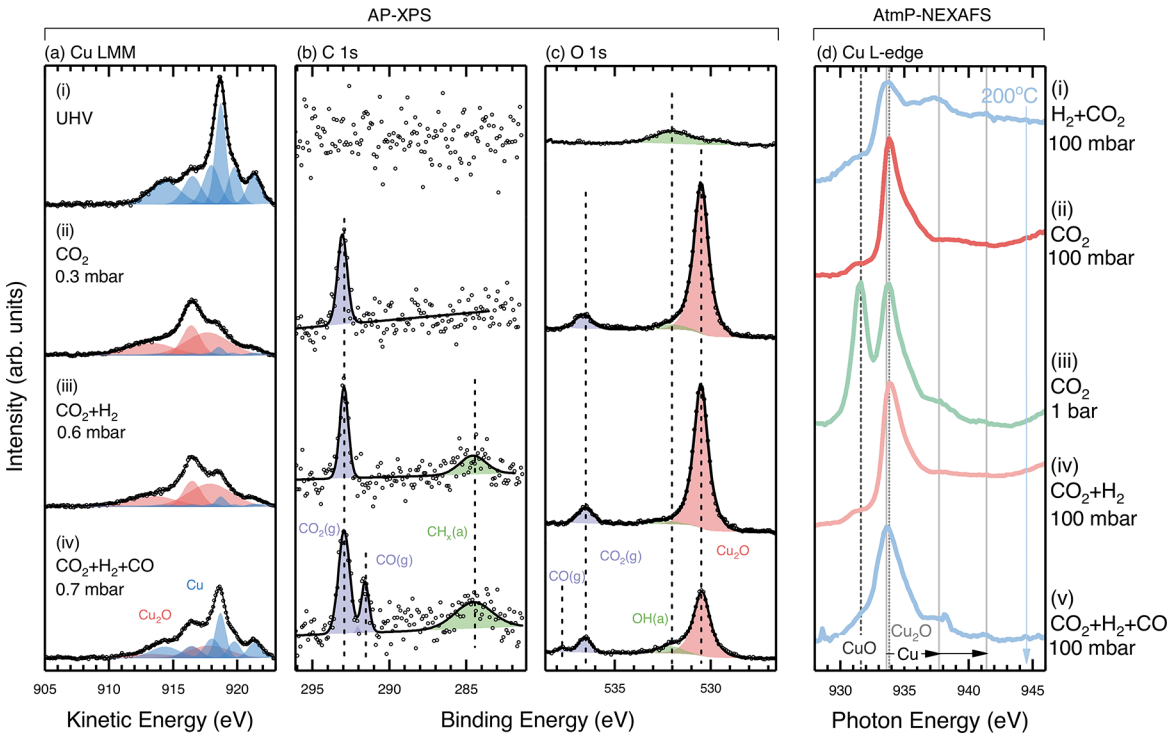

Figure 3. (a–c) Spectra from Cu LMM, C 1s, and O 1s regions acquired (i) in UHV, (ii) 0.3 mbar CO_2, (iii) 0.3 mbar CO_2 and 0.3 mbar H_2, and (iv) 0.3 mbar CO_2, 0.3 mbar H_2 and 0.1 mbar CO. (d) AtmP-NEXAFS spectra from the Cu L_3-edge. Measurements performed at (i) 25 mbar of H_2 and 75 mbar CO_2, (ii) 100 mbar of CO_2, (iii) 1 bar of CO_2, (iv) 50 mbar CO_2 and 50 mbar H_2, and (v) 45 mbar CO_2, 45 mbar H_2 and 10 mbar CO. The temperature was fixed at 200 °C for all measurements shown.

apparent in Figure 3). Gas-phase CO and CO_2 are shown in purple and adsorbed species are shown in green.

Figure 2a(i) displays AES of the cleaned Cu surface under ultrahigh vacuum (UHV), where only peaks related to metallic Cu (blue peaks) are seen. No C species are discernable (Figure 2b(i)), indicating low levels of surface contamination, and a single broad peak is seen in the O 1s spectrum (Figure 2c(i)) at ∼531.5 eV. We tentatively assign this to hydroxylation of the surface, consistent with the binding energy position of OH commonly reported,[31,32] which is typical for polycrystalline surfaces with high-index facets and numerous grain boundaries where trace water vapor from the measurement chamber can adsorb. However, we note that some literature studies have assigned peaks at similar positions to subsurface oxygen species, which may form during preparation of the polycrystalline foil,[33,34] although other literature studies suggest such species to appear at lower binding energies.[35]

Upon dosing 0.3 mbar of H_2 into the measurement environment, there are no apparent changes in the Cu LMM (Figure 2a(ii)) spectrum. A very small increase in peak intensity in the O 1s (Figure 2c(ii)) spectrum is seen. This could be from the additional H_2O introduced upon dosing with H_2 (contamination from gas dosing), increasing the possible OH peak; alternatively, the intensity of subsurface oxygen has previously been suggested to increase under reducing conditions.[33] A slight increase in the intensity at ∼284.3 eV in the C 1s region (Figure 2b(ii)) is assigned to small amounts of surface hydrocarbon contamination, sometimes referred to as adventitious carbon.[31] When only H_2 is present in the gas phase, the Cu surface is expected to dissociate molecular H_2 into chemisorbed hydrogen (H*),[21] which is not readily detectable with XPS.[36] Following the addition of 0.3 mbar of CO_2 to the gas mixture, we still do not observe any major change in the Cu LMM spectrum (Figure 2a(iii)). However, additional peaks emerge in the C 1s (Figure 2b(iii)) and O 1s (Figure 2c(iii)) spectra. Those at ∼293.0 and ∼ 536.5 eV are attributable to CO_2 in the gas phase.[37] Activation of CO_2 is confirmed by the emergence of a peak corresponding to chemisorbed oxygen (O*) at ∼529.6 eV.[17] This indicates dissociative CO_2 adsorption ($CO_2 \rightleftharpoons O^* + CO$) and/or deoxygenation of intermediate species during CO_2 hydrogenation (e.g., $H_2COO^* \rightleftharpoons O^* + H_2CO$, $OH^* + OH^* \rightleftharpoons O^* + H_2O$).[38] The lack of any discernable change in oxidation state in the AES supports the assignment of chemisorbed oxygen as opposed to lattice oxygen of oxidized Cu. A subsequent O 1s measurement 40 min later shows a similar O* intensity confirming a stable surface coverage. This suggests that O* created from ongoing CO_2 activation reacts with H* on the Cu surface to form OH* and H_2O rather than oxidizing the Cu surface.[39] Note that the O 1s peak associated with H_2O is likely to overlap with the OH* component and may mix to form hydrogen-bonded OH–H_2O.[32,40] Gas-phase H_2 therefore appears to play an active role in keeping the surface metallic, with a reasonably small O* peak detected in the O 1s spectrum and no obvious Cu_2O in the Cu LMM spectrum. At this stage, we cannot exclude the alternative explanation that competitive adsorption of hydrogen suppresses CO_2 adsorption such that the supply of O* is insufficient for Cu oxide formation.[41]

Figure 2a(iv)–2c(iv) shows spectra after the addition of 0.1 mbar of CO into the gas mixture. The Cu LMM spectrum (Figure 2a(iv)) is once again unchanged; however, several changes are apparent in the C 1s and O 1s spectra. Alongside the peaks related to gas phase CO at ∼291.6 and ∼537.9 eV, an additional peak emerges in the C 1s region at ∼287.9 eV (Figure 2b(iv)). This could arise from oxygenated hydro-

https://doi.org/10.1021/jacs.2c12728
J. Am. Chem. Soc. 2023, 145, 6730–6740

carbon contaminants,[31] with the corresponding component in the O 1s region convoluted into the larger OH−H_2O peak, although this could also be assigned to formate.[29] Notably, the O* peak in the O 1s spectrum (Figure 2c(iv)) is greatly diminished in intensity relative to the other adsorbed and gas phase peaks when compared to Figure 2c(iii). This decrease is consistent with CO scavenging O* from the catalyst surface to form gas phase CO_2, i.e., shifting the equilibrium of dissociative CO_2 adsorption ($CO_2 \rightleftharpoons O^* + CO$).

To explore this behavior further, we employ AtmP-NEXAFS, where much higher gas partial pressures (>1 bar) are accessible, more closely approaching those used in industrial methanol synthesis. This technique takes advantage of the much greater attenuation lengths of photons to perform measurements through a pressure-resistant SiN_x (100 nm) membrane onto which a Cu (60 nm) catalyst film is deposited. Interface sensitivity (<10 nm) is achieved by measuring the EY signal that arises from electrons escaping the illuminated solid−gas interface.[20]

Figure 2d shows the Cu L_3-edge NEXAFS spectra for similar gas dosing steps as used for the AP-XPS experiments but with partial pressures around two orders of magnitude higher. The as-loaded Cu film, under vacuum, exhibits two strong peaks apparent at ∼931.3 and ∼934.0 eV and two smaller features at higher photon energies (Figure 2d(i)). The first peak is attributable to CuO, which has a distinctly lower energy onset compared to Cu_2O or metallic Cu as it involves a Cu 2p transition to empty 3d states (the Cu in CuO having a $3d^9$ configuration).[42] Cu_2O and metallic Cu have fully occupied 3d bands, so Cu 2p−4s transitions become dominant, giving rise to a higher absorption onset energy.[42] Metallic Cu exhibits distinct resonances (937.6 eV and 941.3 eV) but is also expected to be more step-like in shape.[43] Therefore, the sharp peak at ∼934.0 eV in Figure 2d(i) must originate partly from Cu_2O, which is known to have a strong peak-like absorption onset with similar onset energy to metallic Cu,[43] in line with previous studies.[30,44] Therefore, the as-loaded sample shows contributions from Cu in three different oxidation states. This is attributable to the gradual oxidation of the initially metallic Cu film due to exposure to air, with Cu_2O and CuO forming at the outermost surface whilst the bulk of the film remains metallic.

Figure 2d(ii) shows the Cu film after heating to 220 °C in 50 mbar of H_2. All of the CuO has been reduced, as indicated by the complete absence of the peak at ∼931.3 eV. The peak at ∼934.0 eV remains, as do the resonances at higher energy. These peaks are consistent with a combination of Cu_2O and metallic Cu, indicating that 220 °C is insufficient to fully reduce Cu_2O to Cu in H_2 (50 mbar). Increasing the temperature to 275 °C under the same pressure of H_2 (Figure 2d(iii)) leads to further reduction of the surface yielding, fully metallic Cu, as seen by the step-like spectral shape with a broad absorption onset shifted to slightly lower energy (∼933.7 eV), and the relatively stronger fine structure peaks (∼937.6 and ∼941.3 eV).

After fully reducing the surface to a metallic state, the temperature was lowered to 200 °C, and CO_2 was introduced into the chamber matching the partial pressure of H_2 (50 mbar of CO_2 + 50 mbar H_2). Figure 2d(iv) shows negligible changes to the spectrum acquired, which retains its metallic line shape, confirming that the findings of Figure 2a−c hold at higher pressures. On increasing the partial pressure ratio to 75 mbar CO_2 + 25 mbar H_2 (Figure 2d(v)), the Cu remains predominantly metallic. However, there is a slight weakening of the fine structure peaks and the emergence of a small peak at ∼931.5 eV, indicating that a small amount of Cu_2O and CuO is formed. Therefore, the ratio of H_2 and CO_2 gas is important, with further increases in CO_2 partial pressure expected to yield more oxidation of the Cu surface. Note that in addition to the Cu L_3-edge, C K-edge and O K-edge were also acquired during the AtmP-NEXAFS experiment; however, gas phase peaks from CO_2 and CO (after inclusion in the gas mixture) dominate these spectra.

Figure 3 shows the results of similar AP-XPS and AtmP-NEXAFS experiments but where the order of CO_2 and H_2 introduction is reversed. Prior to the AP-XPS measurements in Figure 3a−c, the Cu surface was cleaned by sputtering and annealing; on the other hand, for AtmP-NEXAFS, the Cu surface was untreated, with the measurements continuing directly from Figure 2. Figure 3a(i) shows the Cu LMM spectrum immediately following the surface preparation. This matches the spectrum seen in Figure 2a, displaying only the features associated with metallic Cu. Similarly, no hydrocarbon contamination is seen in the C 1s spectrum (Figure 3b(i)), and the hydroxyl peak is still visible in the O 1s region (Figure 3c(i)) due to small and unavoidable water vapor contamination in the AP measurement chamber. The slightly higher binding energy of this O 1s peak (∼532.0 eV) compared to Figure 2c(i) (∼531.5 eV) corresponds more closely to surface rather than subsurface oxygen species.[32,34] A small shoulder peak is also seen here at ∼529.5 eV. This may be attributable to a small amount of Cu_2O (not resolvable in the AES), although its lower binding energy and larger FWHM (∼0.5 eV wider) compared to the other Cu_2O peaks indicates that it is more likely related to O* at the surface.[45,46]

Once 0.3 mbar CO_2 is dosed into the chamber (Figure 3a(ii)), the Cu LMM spectrum changes significantly, accompanied by the emergence of an intense peak at ∼530.5 eV in the O 1s region (Figure 3c(ii)). This indicates Cu_2O formation arising from CO_2 dissociation on the surface. Lattice oxygen in Cu_2O was previously reported to produce a peak at around 530.1−530.4 eV;[24,31,45,47] the small shift in position seen here is within experimental error and could be due to variations in binding strength across different crystal orientations on the polycrystalline sample.[48] From the AES, the percentage of Cu_2O can be estimated as ∼85% of the detected signal. Considering the roughly 1 nm inelastic mean free path (IMFP) of the Auger−Meitner electrons, we can estimate the nominal thickness of the oxide layer on the surface to be at least ∼1 nm. Such prominent oxidation of the surface and a few subsurface layers is again consistent with dissociative adsorption of CO_2,[17,39,49] which supplies O* that oxidizes the initially metallic Cu. CO, which also forms due to CO_2 dissociation, is expected to desorb immediately to the gas phase at 200 °C.[50] Thus, no features attributable to adsorbed CO or CO_2 are expected in the C 1s and O 1s spectra of Figure 3b,c(ii), although gas phase CO_2 is still apparent. Similar to the O 1s spectra obtained in vacuum, the surface appears to be partly hydroxylated.

The addition of 0.3 mbar H_2 to the 0.3 mbar CO_2 does not result in any considerable change in the oxidation state of Cu, with an ∼85% oxide ratio still obtained from the Cu LMM spectrum (Figure 3a(iii)) and the relatively intense peak at around ∼530.5 eV persisting (Figure 3c(iii)). Moreover, the addition of H_2 does not change the intensity ratio between the O 1s peaks arising from gaseous CO_2 and lattice Cu_2O. A

https://doi.org/10.1021/jacs.2c12728
J. Am. Chem. Soc. 2023, 145, 6730−6740

hydrocarbon peak does, however, emerge in the C 1s region (Figure 3b(iii)), as also seen when H_2 is present in Figure 2b.

Only after the introduction of 0.1 mbar CO into the gas mixture (Figure 3a(iv)) does the oxide-to-metallic ratio obtained from the Cu LMM spectrum reduce to ∼35%, accompanied by a reduction in the intensity of the Cu_2O peak at ∼530.5 eV (Figure 3c(iv)). The O 1s XPS intensity ratio between lattice oxygen and oxygen in gas-phase CO_2 drops to ∼60% of that without CO present. We thus suggests that CO plays an active role in reducing Cu_2O, making more metallic adsorption sites available by scavenging oxygen on the surface. The XP spectra presented here were acquired within 1 h of the introduction of CO, with longer exposures of >2 h at the same temperature eventually leading to the recovery of metallic Cu to a large extent (data not shown). We note that the peaks attributed to hydrocarbons and hydroxyl groups persist when CO is dosed; however, oxygenated hydrocarbon contaminants are not discernable. Gas phase CO is clearly seen in both the C 1s and O 1s spectra in addition to gas phase CO_2 (Figure 3b(iv),c(iv)).

Figure 3d shows the Cu L_3-edge NEXAFS following on from the experiment displayed in Figure 2d(v), i.e., Figure 2d(v) and Figure 3d(i) are the same spectrum. In order to simulate the gas dosing protocol used for AP-XPS in Figure 3(ii), the flow of H_2 into the cell was stopped, leaving only CO_2 at a pressure of 100 mbar (Figure 3d(ii)). A fairly rapid change from metallic Cu to Cu_2O is observed (measurements performed ∼30 mins apart), with a small contribution from CuO also apparent.

Following this initial change, the pressure of CO_2 was increased to 1 bar (Figure 3d(iii)), where we see significant CuO formation not seen at lower CO_2 pressures. This can be understood as the increase in partial pressure of CO_2 shifting the chemical equilibrium in favor of increased CO_2 dissociation, thereby increasing the supply of O*, which feeds CuO formation. This result highlights the importance of approaching realistic reaction conditions (in this case, high pressures) when studying catalytic reactions, as even under AP conditions, the catalyst state can differ from that seen at higher pressures.

After adding H_2 (50 mbar) back into the gas mixture and returning to a total pressure of 100 mbar (Figure 3d(iv)), we see the removal of most CuO with the Cu_2O peak again dominating; however, no features of metallic Cu are apparent. Only after adding CO into the gas mixture (45 mbar CO_2, 45 mbar H_2, and 10 mbar CO) does the line shape become less asymmetric, and the fine structure peaks of metallic Cu emerge (Figure 3d(v)), indicating partial reduction of the surface. As observed in Figure 3a(iv), at this relatively low ratio of CO, the surface does not become fully metallic; however, some reduction of the surface by CO is seen. CO is thus confirmed to increase the number of metallic sites, which are most catalytically active for H_2 and CO_2 dissociation.

By comparing Figure 2(iv) and Figure 3(iv), our AP-XPS and AtmP-NEXAFS results reveal a significant difference in catalyst oxidation state depending on the order of gas dosing for otherwise identical reaction conditions (1:1 mixture of CO_2:H_2 at either a total pressure of 0.6 mbar (AP-XPS) or 100 mbar (AtmP-NEXAFS)). If thermodynamic equilibrium is reached, then the final state should be independent of the direction of the approach. Here, we find that the Cu surface remains predominantly metallic when H_2 is dosed prior to CO_2 (Figure 2(iv)), even when relatively CO_2-rich conditions are reached (3:1, Figure 2(v)). However, when CO_2 is introduced first, the Cu surface oxidizes toward CuO, with the subsequent addition of H_2 only leading to partial reduction to predominantly Cu_2O (Figure 3(iv)). Even pure H_2 (50 mbar) at 220 °C does not yield a fully metallic Cu surface, with higher temperatures (275 °C) needed to achieve this (see Figure 2d(iii)), indicating a large kinetic barrier for H_2 dissociation on Cu.[51,52] Loosely packed metallic Cu surfaces, on the other hand, dissociate H_2 at a reasonable rate even at room temperature.[21] In this context, when H_2 is dosed first, ongoing H_2 dissociation on the metallic Cu presumably scavenges O* from CO_2 activation to form OH* and H_2O, thereby preventing Cu oxidation.[39,53−55] Given that Cu is found to remain reduced across a wide pressure range (up to 100 mbar) and the presence of O* in AP-XPS measurements confirms ongoing CO_2 activation, the suppression of Cu oxidation by competitive hydrogen adsorption can be largely excluded.

Once the Cu surface is oxidized, the rate of H_2 dissociation becomes very low and insufficient to recover a metallic surface. However, our results confirm that the metallic character is at least partially recovered by the addition of CO, which is more effective at reducing Cu_2O compared to H_2. Dissociation of H_2 is critical to methanol synthesis, and our results here point toward an important role for CO in the gas mixture: as an oxygen scavenger to maintain metallic Cu sites. Maintaining these sites allows both H_2 and CO_2 dissociation to proceed, especially as CO_2 activation tends to rapidly oxidize and deactivate the surface unless O* is continuously removed.[17]

We have so far considered soft X-ray spectroscopy measurements to follow changes in the chemical state of the catalyst surface with gas dosing. To complement these studies, MS was used to observe how the reaction products vary with the order of H_2 and CO_2 dosing. We focus here on the H_2O signal (a product of eqs 1 and 3), noting that the yield of CH_3OH is small for unsupported Cu, and the setup used is not well-optimized for CH_3OH detection (see Figure S1).

Figure 4 shows the H_2O signal generated from the Cu powder over time. Prior to this, the Cu was reduced in H_2 at

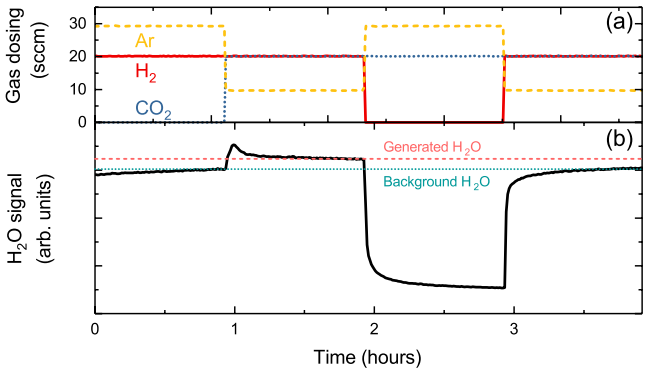

Figure 4. Time evolution of H_2O mass signal for different reaction steps. (a) Flow rates of gases dosed during the reaction. The gas dosing steps proceeded as follows: H_2 (20 sccm), H_2 (20 sccm) and CO_2 (20 sccm), CO_2 (20 sccm), and finally H_2 (20 sccm) and CO_2 (20 sccm). Ar gas was used to balance the chamber pressure and maintain a constant total flow of 50 sccm. (b) H_2O signal during the reaction. The zero of the time scale is set to when the temperature reached 200 °C and the pressure is maintained at 1 bar throughout. At t = 0 h, the Cu is expected to be metallic after having been reduced in H_2 at 275 °C.

https://doi.org/10.1021/jacs.2c12728
J. Am. Chem. Soc. 2023, 145, 6730−6740

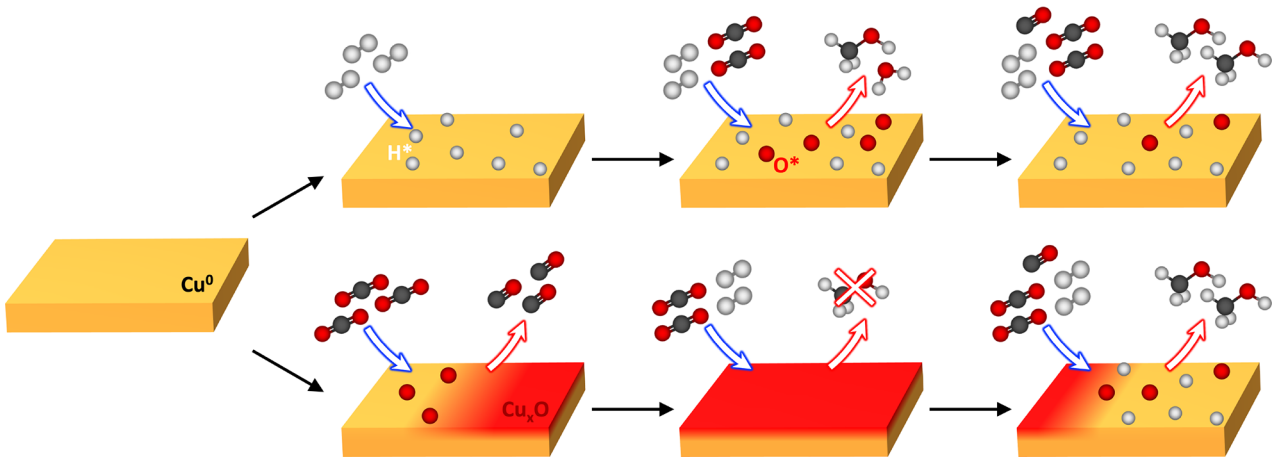

Figure 5. Illustrative diagram of the proposed reaction pathways during exposure of Cu to H_2, CO_2 and CO. The top row corresponds to the gas dosing order in Figure 2, i.e., H_2 first, while the bottom row corresponds to the dosing order in Figure 3, i.e., CO_2 first.

275 °C to yield metallic Cu, as confirmed by the AtmP-NEXAFS and further ex situ characterization (see Figures S4 and S5). During the first hour, a stable H_2O signal is observed while dosing H_2, corresponding to a background level of H_2O arising from residual species from the gas lines/reactor walls. For the second hour, CO_2 is introduced alongside H_2. There is a clear initial increase (peak) in the H_2O signal, which decays and stabilizes at a higher level than the background signal. The initial increase is characteristic of a transient state brought about by the surface reacting to the change in conditions. The higher level at which the H_2O signal equilibrates is attributable to H* (from H_2 dissociation) on the Cu surface reacting with O* and other reaction intermediates (from CO_2 activation) to form H_2O as part of the CO_2 hydrogenation (eq 1) and/or reverse-WGS reactions (eq 3).[38,56] This can also explain the transient behavior, with the steady-state H* coverage stabilized during H_2 exposure serving as a reservoir for reaction with O* when CO_2 is introduced, resulting in an elevated H_2O signal until a new steady-state H* coverage is reached. This further supports the arguments presented above that the reaction of H* with the O* generated by CO_2 activation is primarily responsible for maintaining the Cu surface in a metallic state rather than the suppression of CO_2 adsorption by competitive H* adsorption.

In the third hour of the experiment, H_2 is removed from the gas mixture, and as expected, the H_2O signal drops to a much lower level. During this exposure to CO_2 alone, the surface of the Cu will be oxidized, as confirmed by the AtmP-NEXAFS measurements of Figure 3d(ii, iii). When H_2 is reintroduced into the gas mixture for the fourth hour, the H_2O signal returns to the background level seen when only H_2 is present, and no initial peak associated with a transient state is observed. The lack of additional H_2O formation is consistent with observations from the earlier spectroscopy measurements: a large kinetic barrier to H_2 dissociation exists on Cu_2O, meaning that it is not reduced to metallic Cu by H_2 addition at 200 °C. It also indicates that CO_2 hydrogenation and reverse-WGS reactions are heavily suppressed compared to when H_2 is dosed onto metallic Cu prior to the CO_2. Although the addition of CO is expected to recover the catalytically active metallic sites, this will also cause a shift in the equilibrium of eq 3 suppressing H_2O formation by WGS. Indeed, a slight drop in the H_2O mass signal is observed on CO addition (see Figure S6), consistent with CO providing an additional pathway for O* removal.

Figure 5 summarizes the main reaction pathways revealed by this study when $H_2/CO_2/CO$ gas mixtures react on Cu surfaces. The ratio of H_2 to CO_2 and the order in which they are introduced can significantly alter the catalyst state and its activity toward methanol synthesis reactions.

Starting from an initially metallic catalyst, we find that when H_2 is used as the initial reactant gas, the Cu surface is maintained in a metallic state, with hydrogen acting to remove any residual atomic oxygen from the Cu surface. When CO_2 is introduced into the gas mixture, its activation on the Cu surface is observed through the emergence of chemisorbed atomic oxygen, but without formation of a distinct Cu oxide phase (apart from at high CO_2:H_2 ratios when Cu, Cu_2O, and CuO are found to coexist). This behavior can be accounted for by the ongoing supply of H* through H_2 dissociation, which removes O* produced from CO_2 activation in the form of H_2O vapor, thereby preventing it from oxidizing the surface. This is supported by MS (Figure 4) where the H_2O signal increases when CO_2 is added to the gas mixture. This confirms CO_2 and H_2 activation on the metallic Cu surface, which are both critical to the CO_2 hydrogenation and reverse-WGS reactions that occur under methanol synthesis conditions. Previous literature studies indicate a clear correlation between CO_2 activation and Cu coordination, following the order Cu(110) > Cu(100) > Cu(111) for the low-index surfaces, with reported activation energies for CO_2 dissociation of 0.64−0.67 eV on Cu(110),[49,57] 0.83−0.96 eV on Cu(100),[58,59] and 0.93−1.33 eV on Cu(111).[49,60] Steps are found to be preferential sites for CO_2 dissociation, and their presence may account for some of the lower barriers obtained from experimental studies.[58,60] Activation energies for H_2 dissociation are generally much lower and follow the same order for the low-index surfaces: 0.28 eV on Cu(110),[48] 0.51 eV on Cu(100),[48] 0.54 eV on Cu(111).[61] Therefore, although our samples herein are polycrystalline, these trends are fully consistent with the behavior we observe with the more rapid dissociation of H_2 on metallic Cu able to remove excess O* produced from CO_2 activation.

When the ratio of CO_2:H_2 is increased, a small amount of oxide formation is observed, as in Figure 2d(v). This oxidation can be rationalized by the amount of O* increasing relative to H* on the surface, such that some excess O* does not react

https://doi.org/10.1021/jacs.2c12728
J. Am. Chem. Soc. 2023, 145, 6730−6740

with H* to form H_2O and is thus available to oxidize Cu. The addition of CO has little effect on the chemical state of the already metallic catalyst; however, the concentration of atomic oxygen is significantly reduced on the Cu surface, highlighting the role of CO as an oxygen scavenger.[62] Thus, while CO acts as an oxygen scavenger to maintain a catalytically active surface, this is less crucial when H_2 is dosed prior to CO_2.

On the other hand, if CO_2 is used as the initial reactant gas, then significant oxidation of the Cu surface is observed ($2Cu + O^* \rightleftharpoons Cu_2O$), attributable to O* provided by CO_2 dissociation. CO_2 is found to adsorb as $CO_2^{\delta-}$ on Cu(111) at low pressures (0.01−1 mbar) and room temperature,[17,49] but on more active Cu (100), Cu(110), and stepped surfaces, CO_2 dissociation is observed through the emergence of chemisorbed oxygen[63,64] and is even seen on Cu(111) as pressure and temperature are increased.[49] However, O* coverage blocks further CO_2 adsorption on the catalyst surface leading to "self-poisoning".[17,39,49] Although O* coverages of >0.5 monolayers have been observed on Cu(100) during CO_2 exposure through the breakup of the surface into nanoclusters, the Cu subsurface remains predominantly metallic at room temperature.[17] The greater extent of catalyst oxidation observed on polycrystalline Cu herein is attributable to the higher temperature during CO_2 exposure, with the higher oxygen diffusivity presumably facilitating Cu_2O formation.

At higher CO_2 pressures of 100 mbar and above, we observe the emergence of CuO at the surface ($Cu_2O + O^* \rightleftharpoons 2CuO$), which is an appreciable component at 1 bar. On lowering the CO_2 pressure and introducing H_2, the catalyst reduces again to predominantly Cu_2O, but further reduction to metallic Cu is not observed. We suggest that this is due to a large kinetic barrier for H_2 dissociation on Cu_2O (as previously discussed).[51] Indeed, calculations of H_2 dissociation on oxygen covered Cu surfaces obtained activation energies of 1.06 eV on $O(2 \times 2)/Cu(100)$.[65] This large barrier is also apparent from our AtmP-NEXAFS measurements in Figure 2d(ii, iii), where heating to 220 °C in H_2 (50 mbar) is not sufficient to fully reduce the Cu_2O surface, which only becomes metallic after heating to 275 °C. Our MS results (Figure 4) are also consistent with this, with a similar H_2O signal observed when H_2 is added after CO_2 dosing to when only H_2 is dosed. We note that these findings are broadly consistent with prior DFT calculations suggesting that CuO is easier to reduce than Cu_2O in the presence of H_2.[66]

Although the addition of H_2 after CO_2 does not reduce the surface beyond Cu_2O, we find that further reduction can be achieved by the addition of CO ($Cu_2O + CO \rightleftharpoons 2Cu + CO_2$). CO is thus conclusively shown to behave as an oxygen scavenger, yielding metallic sites that are more catalytically active for CO_2 activation and H_2 dissociation. An overall activation energy of 0.26 eV for the reduction of Cu_2O with CO is reported based on thermogravimetric analysis,[67] while single-crystal AP-XPS studies have determined activation energies for the removal of preadsorbed O on Cu(111) as 0.24 eV, Cu(100) as 0.29 eV, and Cu(110) as 0.51 eV.[46] These are generally well below the corresponding activation barriers for CO_2 dissociation, and while we consider polycrystalline catalyst surfaces herein, this is nevertheless consistent with our observation that a small addition of CO to the reactant feed is sufficient to maintain metallic Cu by the rapid removal of excess O*. Maintaining metallic Cu sites is critical to achieving methanol generation at a significant rate, with an increase in the number of these sites shown to increase activity toward methanol formation.[68] From eq 3, it is also clear that introducing CO shifts the equilibrium making reverse-WGS less favorable such that more CO_2 is directly converted to CH_3OH rather than being converted into CO. Thus, our results demonstrate the importance of using CO in the gas feed for methanol synthesis from CO_2 and H_2 to prevent Cu catalyst deactivation by maintaining metallic sites across a wider range of conditions, including at high CO_2:H_2 ratios.[17]

While our focus herein has been the surface of unsupported Cu catalysts, industrially, ZnO is typically used to support Cu for methanol synthesis. There remains significant debate over the exact nature of the interaction between Cu and ZnO that leads to improved methanol yield.[69−72] However, it is well accepted that in the presence of ZnO, the Cu remains metallic during methanol synthesis.[70,72] Our results highlight the importance of Cu remaining metallic in order to activate H_2 as well as CO_2, and spillover of H* to ZnO has been implicated in the formation of reactive intermediates.[70] There has been much recent discussion on the nature of reduced Zn species and the intermediates responsible for the promotional effect of ZnO supports; for example, the formation of a CuZn alloy is often considered, but this requires highly reducing conditions.[69,71,72] The inclusion of CO has been shown to help maintain such a CuZn alloy,[72] playing a similar role of oxygen scavenger as observed herein, albeit promoting the reduction of different species (since the presence of Zn already maintains metallic Cu). Hence, the precise role of CO may depend critically on the catalyst composition used.

CONCLUSIONS

In summary, we have shown how the surface chemical state and absorbates present on Cu vary with the order of gas dosing during CO_2 and H_2 exposure at temperatures typically used for methanol synthesis. We note that through our complementary AP-XPS and AtmP-NEXAFS study, the understanding developed is extended to the atmospheric pressure regime while still providing surface-sensitive information through soft X-ray spectroscopic techniques. This combined approach proves a practical avenue for studying catalytic reactions at industrially relevant gas pressures. We find that the Cu surface remains metallic in the presence of CO_2 and H_2, when H_2 is dosed first. CuO is observed at high CO_2 ratios; however, Cu retains the significant metallic character needed for ongoing CO_2 and H_2 activation. When CO_2 is dosed prior to H_2, the Cu surface readily oxidizes to Cu_2O, with significant CuO formation at high CO_2 pressures. The introduction of H_2 only returns the surface to Cu_2O with further reduction suppressed due to a high kinetic barrier for H_2 dissociation. The addition of CO to the gas feed is found to scavenge oxygen from the Cu surface, thus making metallic Cu sites available for CO_2 and H_2 activation. Hence, even though CO_2 has been established as the carbon source for methanol generation,[12] this study demonstrates the importance of including CO in the reactant mixture. This contributes to a process that is more robust to variations in reaction conditions, particularly given that large kinetic barriers for certain processes (e.g., H_2 activation) can lead to effective catalyst deactivation if the desired oxidation state is lost. Our results highlight the importance of studying these phenomena at pressures close to realistic industrial conditions, as this can alter both the equilibrium and reaction kinetics.

https://doi.org/10.1021/jacs.2c12728
J. Am. Chem. Soc. 2023, 145, 6730−6740

■ ASSOCIATED CONTENT

Supporting Information

The Supporting Information is available free of charge at https://pubs.acs.org/doi/10.1021/jacs.2c12728.

Microstructural and chemical characterization of the Cu catalyst variants; time evolution of H_2O and CH_3OH MS signals for different reaction steps (PDF)

■ AUTHOR INFORMATION

Corresponding Authors

Baran Eren − *Department of Chemical and Biological Physics, Weizmann Institute of Science, 76100 Rehovot, Israel;* orcid.org/0000-0002-0521-8127; Email: baran.eren@weizmann.ac.il

Robert S. Weatherup − *Department of Materials, University of Oxford, Oxfordshire OX1 3PH, U.K.; Diamond Light Source, Oxfordshire OX11 0DE, U.K.;* orcid.org/0000-0002-3993-9045; Email: robert.weatherup@materials.ox.ac.uk

Authors

Jack E. N. Swallow − *Department of Materials, University of Oxford, Oxfordshire OX1 3PH, U.K.*

Elizabeth S. Jones − *Department of Materials, University of Oxford, Oxfordshire OX1 3PH, U.K.*

Ashley R. Head − *Center for Functional Nanomaterials, Brookhaven National Laboratory, Upton 11973 New York, United States;* orcid.org/0000-0001-8733-0165

Joshua S. Gibson − *Department of Materials, University of Oxford, Oxfordshire OX1 3PH, U.K.*

Roey Ben David − *Department of Chemical and Biological Physics, Weizmann Institute of Science, 76100 Rehovot, Israel*

Michael W. Fraser − *Department of Materials, University of Oxford, Oxfordshire OX1 3PH, U.K.*

Matthijs A. van Spronsen − *Diamond Light Source, Oxfordshire OX11 0DE, U.K.;* orcid.org/0000-0002-5136-2816

Shaojun Xu − *Catalysis Hub, Oxfordshire OX11 0FA, U.K.;* orcid.org/0000-0002-8026-8714

Georg Held − *Diamond Light Source, Oxfordshire OX11 0DE, U.K.;* orcid.org/0000-0003-0726-4183

Complete contact information is available at: https://pubs.acs.org/10.1021/jacs.2c12728

Notes

The authors declare no competing financial interest.

The authors confirm that the data supporting the findings of this study are available within the article and its supplementary materials.

■ ACKNOWLEDGMENTS

This project has received funding from the European Research Council (ERC) under the European Union's Horizon 2020 research and innovation programme (EXISTAR, grant agreement No. 950598). We acknowledge support from the Engineering and Physical Science Research Council (EPSRC) through grants EP/T001038/1 and EP/R010145/1 (Henry Royce Institute). E.S.J. acknowledges a Clarendon Scholarship. B.E. and R.S.W. are grateful to the Weizmann − UK Making Connections Programme. R.S.W. acknowledges a CAMS-UK Fellowship through the Analytical Chemistry Trust Fund and a UKRI Future Leaders Fellowship (MR/V024558/1). We thank Diamond Light Source for beamtime on Beamline B07 under proposal SI25834-2 and are particularly grateful to Andrew Watts for technical support throughout this experiment. We thank Dr. Phani Karamched of the David Cockayne Centre for Electron Microscopy for assistance with EBSD and SEM. The authors would like to thank RCaH and the UK Catalysis Hub for access to equipment and associated support. This research used the Proximal Probes Facility of the Center for Functional Nanomaterials (CFN), which is a U.S. Department of Energy Office of Science User Facility, at Brookhaven National Laboratory under Contract No. DE-SC0012704.

■ ABBREVIATIONS

AES	Auger−Meitner electron spectroscopy
AP	ambient pressure
EBSD	electron backscatter diffraction
MS	mass spectrometry
NEXAFS	near edge X-ray absorption fine structure
SEM	scanning electron microscopy
WGS	water gas shift
XAS	X-ray absorption spectroscopy
XPS	X-ray photoelectron spectroscopy

■ REFERENCES

(1) Ali, K. A.; Abdullah, A. Z.; Mohamed, A. R. Recent Development in Catalytic Technologies for Methanol Synthesis from Renewable Sources: A Critical Review. *Renewable Sustainable Energy Rev.* **2015**, *44*, 508−518.

(2) Methanol Market Services Asia. *Global Methanol Supply and Demand Summary*; https://www.methanol.org/methanol-price-supply-demand (accessed Nov 28, 2022).

(3) Olah, G. A. Towards Oil Independence through Renewable Methanol Chemistry. *Angew. Chem., Int. Ed.* **2013**, *52*, 104−107.

(4) Olah, G. A. Beyond Oil and Gas: The Methanol Economy. *Angew. Chem., Int. Ed.* **2005**, *44*, 2636−2639.

(5) Goeppert, A.; Czaun, M.; Jones, J. P.; Surya Prakash, G. K.; Olah, G. A. Recycling of Carbon Dioxide to Methanol and Derived Products-Closing the Loop. *Chem. Soc. Rev.* **2014**, *43*, 7995−8048.

(6) Dalena, F.; Senatore, A.; Marino, A.; Gordano, A.; Basile, M.; Basile, A. *Methanol Production and Applications: An Overview*; Elsevier B.V., 2018.

(7) Behrens, M.; Studt, F.; Kasatkin, I.; Kühl, S.; Hävecker, M.; Abild-pedersen, F.; Zander, S.; Girgsdies, F.; Kurr, P.; Kniep, B.; et al. The Active Site of Methanol Synthesis over $Cu/ZnO/Al_2O_3$ Industrial Catalysts. *Science* **2012**, *759*, 893−898.

(8) Frost, J. C. Junction Effect Interactions in Methanol Synthesis Catalysts. *Nature* **1988**, *334*, 577−580.

(9) Behrens, M. Heterogeneous Catalysis of CO_2 Conversion to Methanol on Copper Surfaces. *Angew. Chem., Int. Ed.* **2014**, *53*, 12022−12024.

(10) Pontzen, F.; Liebner, W.; Gronemann, V.; Rothaemel, M.; Ahlers, B. CO_2-Based Methanol and DME - Efficient Technologies for Industrial Scale Production. *Catal. Today* **2011**, *171*, 242−250.

(11) Kamsuwan, T.; Krutpijit, C.; Praserthdam, S.; Phatanasri, S.; Jongsomjit, B.; Praserthdam, P. Comparative Study on the Effect of Different Copper Loading on Catalytic Behaviors and Activity of $Cu/ZnO/Al_2O_3$ Catalysts toward CO and CO_2 Hydrogenation. *Heliyon* **2021**, *7*, No. e07682.

(12) Chinchen, G. C.; Denny, P. J.; Parker, D. G.; Spencer, M. S.; Whan, D. A. Mechanism of Methanol Synthesis from $CO_2/CO/H_2$ Mixtures over Copper/Zinc Oxide/Alumina Catalysts: Use of ^{14}C-Labelled Reactants. *Appl. Catal.* **1987**, *30*, 333−338.

(13) Nielsen, N. D.; Jensen, A. D.; Christensen, J. M. The Roles of CO and CO_2 in High Pressure Methanol Synthesis over Cu-Based Catalysts. *J. Catal.* **2021**, *393*, 324−334.

(14) Nielsen, N. D.; Thrane, J.; Jensen, A. D.; Christensen, J. M. Bifunctional Synergy in CO Hydrogenation to Methanol with Supported Cu. *Catal. Lett.* **2020**, *150*, 1427−1433.
(15) Nerlov, J.; Chorkendorff, I. Methanol Synthesis from CO_2, CO, and H_2 over Cu(100) and Ni/Cu(100). *J. Catal.* **1999**, *181*, 271−279.
(16) Rozovskii, A. Y.; Lin, G. I. Fundamentals of Methanol Synthesis and Decomposition. *Top. Catal.* **2003**, *22*, 137−150.
(17) Eren, B.; Weatherup, R. S.; Liakakos, N.; Somorjai, G. A.; Salmeron, M. B. Dissociative Carbon Dioxide Adsorption and Morphological Changes on Cu(100) and Cu(111) at Ambient Pressures. *J. Am. Chem. Soc.* **2016**, *138*, 8207−8211.
(18) Weatherup, R. S.; Eren, B.; Hao, Y.; Bluhm, H.; Salmeron, M. B. Graphene Membranes for Atmospheric Pressure Photoelectron Spectroscopy. *J. Phys. Chem. Lett.* **2016**, *7*, 1622−1627.
(19) Weatherup, R. S. 2D Material Membranes for Operando Atmospheric Pressure Photoelectron Spectroscopy. *Top. Catal.* **2018**, *61*, 2085−2102.
(20) Jones, E. S.; Swallow, J. E. N.; Weatherup, R. S. Enclosed Cells for Extending Soft X-Ray Spectroscopies to Atmospheric Pressures and Above. *ACS Symp. Ser.* **2021**, *1396*, 175−218.
(21) Österlund, L.; Rasmussen, P. B.; Thostrup, P.; Lægsgaard, E.; Stensgaard, I.; Besenbacher, F. Bridging the Pressure Gap in Surface Science at the Atomic Level: H/Cu(110). *Phys. Rev. Lett.* **2001**, *86*, 460−463.
(22) Eren, B.; Zherebetskyy, D.; Patera, L. L.; Wu, C. H.; Bluhm, H.; Africh, C.; Wang, L. W.; Somorjai, G. A.; Salmeron, M. Activation of Cu(111) Surface by Decomposition into Nanoclusters Driven by CO Adsorption. *Science* **2016**, *351*, 475−478.
(23) Eads, C. N.; Zhong, J. Q.; Kim, D.; Akter, N.; Chen, Z.; Norton, A. M.; Lee, V.; Kelber, J. A.; Tsapatsis, M.; Boscoboinik, J. A.; et al. Multi-Modal Surface Analysis of Porous Films under Operando Conditions. *AIP Adv.* **2020**, *10*, 1−10.
(24) Biesinger, M. C. Advanced Analysis of Copper X-Ray Photoelectron Spectra. *Surf. Interface Anal.* **2017**, *49*, 1325−1334.
(25) Fairley, N.; Fernandez, V.; Richard-Plouet, M.; Guillot-Deudon, C.; Walton, J.; Smith, E.; Flahaut, D.; Greiner, M.; Biesinger, M.; Tougaard, S.; et al. Systematic and Collaborative Approach to Problem Solving Using X-Ray Photoelectron Spectroscopy. *Appl. Surf. Sci. Adv.* **2021**, *5*, No. 100112.
(26) Grinter, D. C.; Venturini, F.; Ferrer, P.; van Spronsen, M. A.; Arrigo, R.; Quevedo Garzon, W.; Roy, K.; Large, A. I.; Kumar, S.; Held, G. The Versatile Soft X-Ray (VerSoX) Beamline at Diamond Light Source. *Synchrotron Radiat. News* **2022**, *35*, 39−47.
(27) Held, G.; Venturini, F.; Grinter, D. C.; Ferrer, P.; Arrigo, R.; Deacon, L.; Garzon, W. Q.; Roy, K.; Large, A.; Stephens, C.; et al. Ambient-Pressure Endstation of the Versatile Soft X-Ray (VerSoX) Beamline at Diamond Light Source. *J. Synchrotron Radiat.* **2020**, *27*, 1153−1166.
(28) Tamenori, Y. Electron Yield Soft X-Ray Photoabsorption Spectroscopy under Normal Ambient-Pressure Conditions. *J. Synchrotron Radiat.* **2013**, *20*, 419−425.
(29) Eren, B.; Sole, C. G.; Lacasa, J. S.; Grinter, D.; Venturini, F.; Held, G.; Esconjauregui, C. S.; Weatherup, R. S. Identifying the Catalyst Chemical State and Adsorbed Species during Methanol Conversion on Copper Using Ambient Pressure X-Ray Spectroscopies. *Phys. Chem. Chem. Phys.* **2020**, *22*, 18806−18814.
(30) Jiang, P.; Prendergast, D.; Borondics, F.; Porsgaard, S.; Giovanetti, L.; Pach, E.; Newberg, J.; Bluhm, H.; Besenbacher, F.; Salmeron, M. Experimental and Theoretical Investigation of the Electronic Structure of Cu_2O and CuO Thin Films on Cu(110) Using x-Ray Photoelectron and Absorption Spectroscopy. *J. Chem. Phys.* **2013**, *138*, No. 024704.
(31) Trotochaud, L.; Head, A. R.; Pletincx, S.; Karslloğlu, O.; Yu, Y.; Waldner, A.; Kyhl, L.; Hauffman, T.; Terryn, H.; Eichhorn, B.; et al. Water Adsorption and Dissociation on Polycrystalline Copper Oxides: Effects of Environmental Contamination and Experimental Protocol. *J. Phys. Chem. B* **2018**, *122*, 1000−1008.
(32) Andersson, K.; Ketteler, G.; Bluhm, H.; Yamamoto, S.; Ogasawara, H.; Pettersson, L. G. M.; Salmeron, M.; Nilsson, A. Autocatalytic Water Dissociation on Cu(110) at near Ambient Conditions. *J. Am. Chem. Soc.* **2008**, *130*, 2793−2797.
(33) Eilert, A.; Cavalca, F.; Roberts, F. S.; Osterwalder, J.; Liu, C.; Favaro, M.; Crumlin, E. J.; Ogasawara, H.; Friebel, D.; Pettersson, L. G. M.; et al. Subsurface Oxygen in Oxide-Derived Copper Electrocatalysts for Carbon Dioxide Reduction. *J. Phys. Chem. Lett.* **2017**, *8*, 285−290.
(34) Bluhm, H.; Hävecker, M.; Knop-Gericke, A.; Kleimenov, E.; Schlögl, R.; Teschner, D.; Bukhtiyarov, V. I.; Ogletree, D. F.; Salmeron, M. Methanol Oxidation on a Copper Catalyst Investigated Using in Situ X-Ray Photoelectron Spectroscopy. *J. Phys. Chem. B* **2004**, *108*, 14340−14347.
(35) Favaro, M.; Xiao, H.; Cheng, T.; Goddard, W. A.; Crumlin, E. J. Subsurface Oxide Plays a Critical Role in CO_2 Activation by Cu(111) Surfaces to Form Chemisorbed CO_2, the First Step in Reduction of CO_2. *Proc. Natl. Acad. Sci. U. S. A.* **2017**, *114*, 6706−6711.
(36) Zhong, J. Q.; Wang, M.; Hoffmann, W. H.; Van Spronsen, M. A.; Lu, D.; Boscoboinik, J. A. Synchrotron-Based Ambient Pressure X-Ray Photoelectron Spectroscopy of Hydrogen and Helium. *Appl. Phys. Lett.* **2018**, *112*, 1−5.
(37) Avval, T. G.; Chatterjee, S.; Bahr, S.; Dietrich, P.; Meyer, M.; Thißen, A.; Linford, M. R. Carbon Dioxide Gas, CO_2(g), by near-Ambient Pressure XPS. *Surf. Sci. Spectra* **2019**, *26*, No. 014022.
(38) Zhao, Y. F.; Yang, Y.; Mims, C.; Peden, C. H. F.; Li, J.; Mei, D. Insight into Methanol Synthesis from CO_2 Hydrogenation on Cu(1 1 1): Complex Reaction Network and the Effects of H2O. *J. Catal.* **2011**, *281*, 199−211.
(39) Qi, S. C.; Liu, X. Y.; Zhu, R. R.; Xue, D. M.; Liu, X. Q.; Sun, L. B. Causation of Catalytic Activity of Cu-ZnO for CO_2 Hydrogenation to Methanol. *Chem. Eng. J.* **2022**, *430*, No. 132784.
(40) Yamamoto, S.; Bluhm, H.; Andersson, K.; Ketteler, G.; Ogasawara, H.; Salmeron, M.; Nilsson, A. In Situ X-Ray Photoelectron Spectroscopy Studies of Water on Metals and Oxides at Ambient Conditions. *J. Phys. Condens. Matter* **2008**, *20*, No. 184025.
(41) Tissot, H.; Wang, C.; Stenlid, J. H.; Panahi, M.; Kaya, S.; Soldemo, M.; Ghadami Yazdi, M.; Brinck, T.; Weissenrieder, J. Interaction of Atomic Hydrogen with the Cu_2O(100) and (111) Surfaces. *J. Phys. Chem. C* **2019**, *123*, 22172−22180.
(42) Grioni, M.; Goedkoop, J. B.; Schoorl, R.; de Groot, F. M. F.; Fuggle, J. C.; Schäfers, F.; Koch, E. E.; Rossi, G.; Esteva, J.-M.; Karnatak, R. C. Studies of Copper Valence States with Cu L_3 X-Ray-Absorption Spectroscopy. *Phys. Rev. B* **1989**, *39*, 1541−1545.
(43) Grioni, M.; Acker, J. F. van; Czyzyk, M. T.; Fuggle, J. C. Unoccupied Electronic Structure and Core-Hole Effects in the x-Ray Absorption Spectra of Cu_2O. *Phys. Rev. B* 1992, *45*, 3309−3318 DOI: 10.1103/PhysRevB.45.3309.
(44) Kvashnina, K. O.; Butorin, S. M.; Modin, A.; Werme, L.; Nordgren, J.; Guo, J. H.; Berger, R. Electronic Structure of Complex Copper Systems Probed by Resonant Inelastic X-Ray Scattering at Cu L_3 Edge. *Phys. B* **2009**, *404*, 3559−3566.
(45) Eren, B.; Heine, C.; Bluhm, H.; Somorjai, G. A.; Salmeron, M. Catalyst Chemical State during CO Oxidation Reaction on Cu(111) Studied with Ambient-Pressure X-Ray Photoelectron Spectroscopy and Near Edge X-Ray Adsorption Fine Structure Spectroscopy. *J. Am. Chem. Soc.* **2015**, *137*, 11186−11190.
(46) Eren, B.; Lichtenstein, L.; Wu, C. H.; Bluhm, H.; Somorjai, G. A.; Salmeron, M. Reaction of CO with Preadsorbed Oxygen on Low-Index Copper Surfaces: An Ambient Pressure X-Ray Photoelectron Spectroscopy and Scanning Tunneling Microscopy Study. *J. Phys. Chem. C* **2015**, *119*, 14669−14674.
(47) Liu, B. H.; Huber, M.; van Spronsen, M. A.; Salmeron, M.; Bluhm, H. Ambient Pressure X-Ray Photoelectron Spectroscopy Study of Room-Temperature Oxygen Adsorption on Cu(1 0 0) and Cu(1 1 1). *Appl. Surf. Sci.* **2021**, *2022*, No. 152438.
(48) Higham, M. D.; Higham, M. D.; Quesne, M. G.; Quesne, M. G.; Catlow, C. R. A.; Catlow, C. R. A.; Catlow, C. R. A. Mechanism of CO2conversion to Methanol over Cu(110) and Cu(100) Surfaces. *Dalton Trans.* **2020**, *49*, 8478−8497.

(49) Yang, T.; Gu, T.; Han, Y.; Wang, W.; Yu, Y.; Zang, Y.; Zhang, H.; Mao, B.; Li, Y.; Yang, B.; et al. Surface Orientation and Pressure Dependence of CO_2 Activation on Cu Surfaces. *J. Phys. Chem. C* **2020**, *124*, 27511−27518.
(50) Vollmer, S.; Witte, G.; Wöll, C. Determination of Site Specific Adsorption Energies of CO on Copper. *Catal. Lett.* **2001**, *77*, 97−101.
(51) Kim, J. Y.; Rodriguez, J. A.; Hanson, J. C.; Frenkel, A. I.; Lee, P. L. Reduction of CuO and Cu_2O with H_2: H Embedding and Kinetic Effects in the Formation of Suboxides. *J. Am. Chem. Soc.* **2003**, *125*, 10684−10692.
(52) Schulz, K. H.; Cox, D. F. Surface Hydride Formation on a Metal Oxide Surface: The Interaction of Atomic Hydrogen with $Cu_2O(100)$. *Surf. Sci.* **1992**, *278*, 9−18.
(53) Grabow, L. C.; Mavrikakis, M. Mechanism of Methanol Synthesis on Cu through CO_2 and CO Hydrogenation. *ACS Catal.* **2011**, *1*, 365−384.
(54) Etim, U. J.; Song, Y.; Zhong, Z. Improving the Cu/ZnO-Based Catalysts for Carbon Dioxide Hydrogenation to Methanol, and the Use of Methanol As a Renewable Energy Storage Media. *Front. Earth Sci.* **2020**, *8*, 1−26.
(55) Yang, Y.; Evans, J.; Rodriguez, J. A.; White, M. G.; Liu, P. Fundamental Studies of Methanol Synthesis from CO_2 Hydrogenation on Cu(111), Cu Clusters, and Cu/ZnO(0001). *Phys. Chem. Chem. Phys.* **2010**, *12*, 9909−9917.
(56) Lim, H. W.; Park, M. J.; Kang, S. H.; Chae, H. J.; Bae, J. W.; Jun, K. W. Modeling of the Kinetics for Methanol Synthesis Using $Cu/ZnO/Al_2O3/ZrO_2$ Catalyst: Influence of Carbon Dioxide during Hydrogenation. *Ind. Eng. Chem. Res.* **2009**, *48*, 10448−10455.
(57) Nakamura, J.; Rodriguez, J. A.; Campbell, C. T. Does CO_2 Dissociatively Adsorb on Cu Surfaces? *J. Phys. Condens. Matter* **1989**, *1*, SB149.
(58) Hagman, B.; Posada-Borbón, A.; Schaefer, A.; Shipilin, M.; Zhang, C.; Merte, L. R.; Hellman, A.; Lundgren, E.; Grönbeck, H.; Gustafson, J. Steps Control the Dissociation of CO_2 on Cu(100). *J. Am. Chem. Soc.* **2018**, *140*, 12974−12979.
(59) Taylor, P. A.; Rasmussen, P. B.; Chorkendorff, I.; Taylor, P. A.; Rasmussen, P. B.; Chorkendorff, I. Carbon Dioxide Chemistry on Cu (100). *J. Vac. Sci. Technol. A Vacuum, Surfaces, Film.* **1992**, *10*, 2570−2575.
(60) Muttaqien, F.; Hamamoto, Y.; Inagaki, K.; Morikawa, Y. Dissociative Adsorption of CO_2 on Flat, Stepped, and Kinked Cu Surfaces. *J. Chem. Phys.* **2014**, *141*, No. 034702.
(61) Gokhale, A. A.; Dumesic, J. A.; Mavrikakis, M. On the Mechanism of Low-Temperature Water Gas Shift Reaction on Copper. *J. Am. Chem. Soc.* **2008**, *130*, 1402−1414.
(62) Szanyi, J.; Goodman, D. W. Methanol Synthesis on a Cu(100) Catalyst. *Catal. Lett.* **1991**, *10*, 383−390.
(63) Fu, S. S.; Somorjai, G. A. Interactions of O_2, CO, CO_2, and D_2 with the Stepped CU(311) Crystal Face: Comparison to Cu(110). *Surf. Sci.* **1992**, *262*, 68−76.
(64) Bönicke, I. A.; Kirstein, W.; Thieme, F. A Study on CO_2 Dissociation on a Stepped (332) Copper Surface. *Surf. Sci.* **1994**, *307−309*, 177−181.
(65) Sakong, S.; Groß, A. Dissociative Adsorption of Hydrogen on Strained Cu Surfaces. *Surf. Sci.* **2003**, *525*, 107−118.
(66) Maimaiti, Y.; Nolan, M.; Elliott, S. D. Reduction Mechanisms of the CuO(111) Surface through Surface Oxygen Vacancy Formation and Hydrogen Adsorption. *Phys. Chem. Chem. Phys.* **2014**, *16*, 3036−3046.
(67) Goldstein, E. A.; Mitchell, R. E. Chemical Kinetics of Copper Oxide Reduction with Carbon Monoxide. *Proc. Combust. Inst.* **2011**, *33*, 2803−2810.
(68) Yoshihara, J.; Campbell, C. T. Methanol Synthesis and Reverse Water-Gas Shift Kinetics over Cu(110) Model Catalysts: Structural Sensitivity. *J. Catal.* **1996**, *161*, 776−782.
(69) Beck, A.; Zabilskiy, M.; Newton, M. A.; Safonova, O.; Willinger, M. G.; van Bokhoven, J. A. Following the Structure of Copper-Zinc-Alumina across the Pressure Gap in Carbon Dioxide Hydrogenation. *Nat. Catal.* **2021**, *4*, 488−497.
(70) Zabilskiy, M.; Sushkevich, V. L.; Palagin, D.; Newton, M. A.; Krumeich, F.; van Bokhoven, J. A. The Unique Interplay between Copper and Zinc during Catalytic Carbon Dioxide Hydrogenation to Methanol. *Nat. Commun.* **2020**, *11*, 1−8.
(71) Divins, N. J.; Kordus, D.; Timoshenko, J.; Sinev, I.; Zegkinoglou, I.; Bergmann, A.; Chee, S. W.; Widrinna, S.; Karslıoğlu, O.; Mistry, H.; et al. Operando High-Pressure Investigation of Size-Controlled CuZn Catalysts for the Methanol Synthesis Reaction. *Nat. Commun.* **2021**, *12*, 1−10.
(72) Amann, P.; Klötzer, B.; Degerman, D.; Köpfle, N.; Götsch, T.; Lömker, P.; Rameshan, C.; Ploner, K.; Bikaljevic, D.; Wang, H.; Soldemo, M.; Shipilin, M.; Goodwin, C. M.; Gladh, J.; Halldin Stenlid, J.; Börner, M.; Schlueter, C.; Nilsson, A. The State of Zinc in Methanol Synthesis over a Zn/ZnO/Cu(211) Model Catalyst. *Science* **2022**, *376*, 603−608.

https://doi.org/10.1021/jacs.2c12728
J. Am. Chem. Soc. 2023, 145, 6730−6740